Spectral Signatures for Identifying Explosives With Wideband Millimeter-Wave Illumination

James C. Weatherall, Jeffrey Barber, and Barry T. Smith

***Abstract*—Millimeter-wave imaging systems used in airports, government buildings, and other facilities for personnel screening use advanced imaging technology (AIT) to detect explosives and weapons concealed under clothing. Additional information in the imaging data can be applied to identify the composition of the detected objects. The method described here demonstrates that material data in the form of the dielectric constant can be derived from the variation of reflectivity in millimeter waves over a range of frequencies from 18 to 40 GHz. By fitting the reflectivity to an optical model, the thickness and dielectric constant, including attenuation, can be computed. The method is applied to samples of inert substances and a military sheet explosive to show that detected anomalies can be distinguished as distinct materials through their dielectric constants. For absorptive materials, a frequency band of lower frequencies, 2–18 GHz, can be applied to detect the dielectric, as is demonstrated in the case of a commercial explosive. Used with AIT, the technique can facilitate the evaluation of threats at personnel checkpoints.**

***Index Terms*—Dielectric detection, explosives, measurement algorithms, millimeter-wave imaging, parameter extraction, reflectometry, weapons detection.**

I. Introduction

ADVANCED imaging technology (AIT) systems used to screen people for concealed explosives and weapons employ millimeter-wave imaging, together with computational algorithms, to identify the presence of threat objects and where they are located on the person. We show that measuring the reflection coefficient over a range of centimeter and millimeter wavelength electromagnetic radiation also provides identifying information on threat objects in the form of dielectric constant. As examples, we detect three types of targets across 22 GHz of bandwidth centered at 29 GHz, in a configuration that is idealized to what is encountered in a screening environment. The data is extracted by a numerical fitting of reflectivity as a function of frequency to a theoretical model based on geometric optics, which obtains both the dielectric constant and the thickness of the target. Unlike standard reflection measurement algorithms [1], [2], this method does not require prior knowledge of the material thickness. Spectral fitting is used for dielectric detection in optical coherence tomography (FD-OCT [3]) for imaging thin lossless media, and multiple frequencies are used to refine transmission scattering measurement of permittivity in low-loss materials [4]. In our adaptation, a large bandwidth exploits the fact that absorption of radiation varies over frequency even with a constant dielectric function [5], [6]. The phase ambiguity that attends reflection-only one-port measurement [7] is solved by the spectral fitting. Free-space reflectometry using horn antennas and metal-backed samples is formulated by [8]–[11]. Dielectric characterizations in multilayered structures have been studied from reflection and transmission data in waveguide [12], [13] and free-space [14], [15]. The implementation of various fitting algorithms to the poorly constrained problem of frequency-dependent multilayer transmission and reflection is made in [13] and [15] with the inclusion of air gaps as layers. Our use of the technique anticipates using an imaging system as the measurement apparatus[16], [17]. The frequency-domain fitting provides more information than the detection of layered anomalies in images from time-domain features [18], [19]. While current AIT imaging systems operate in bands that may be too narrow for this application, i.e., 24–30 GHz [20], [21], future imaging systems will likely expand usage of the millimeter-wave spectrum as sources and sensors continue to develop.

This paper is organized as follows. Section II gives details of the experimental setup and the reflection coefficient modeling. Section III presents measured results on the three materials, estimation of detection error from various effects, and the discriminative value of the detection. Section IV extends the results to other frequency bands and other types of explosives. The application of the technique to imaging systems is discussed in Section V. The conclusion is made in Section VI.

II. Experiment

A. Experimental Setup

Data collection is performed using an 18–40-GHz wideband horn (Q-par WBH18–40) with a vector network analyzer (Agilent N5245A) to collect reflection data in the polar form of the S_{11} parameter. The experimental setup has the sample just beyond the near-field Fraunhofer zone at a distance of 34.5 cm such that the optics are suitable for plane-wave analysis, and the majority of the beam passes through the sample. The small transverse beam size also reduces the variation in phase across the target illumination due to nonparallel ray paths. The samples

Manuscript received June 09, 2015; revised October 29, 2015 and December 30, 2015; accepted December 30, 2015. Date of publication January 29, 2016; date of current version March 03, 2016. This work was supported by the DHS under Contract HSHQDC-15-J-00395 and Contract HSHQDC-13-J-00209.

J. C. Weatherall and J. Barber are with the Battelle Memorial Institute, Egg Harbor Township, NJ 08234 USA (e-mail: james.weatherall@associates.dhs.gov).

B. T. Smith is with the U.S. Department of Homeland Security, Science and Technology Directorate, Transportation Security Laboratory, William J. Hughes Technical Center, Atlantic City International Airport, Atlantic City, NJ 08405 USA.

Color versions of one or more of the figures in this paper are available online at http://ieeexplore.ieee.org.

Digital Object Identifier 10.1109/TMTT.2016.2518159

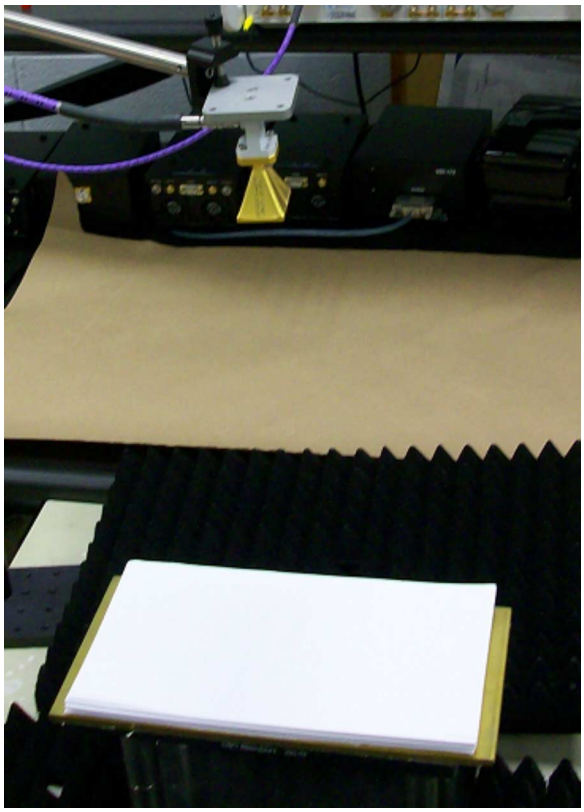

Fig. 1. Measurement setup showing paper sample.

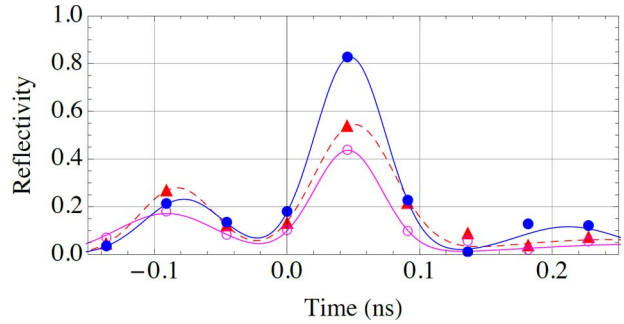

Fig. 2. Time domain of pulsed reflection amplitude: Lexan (filled circle), paper (open circles), and P1000 (triangles). Lines are fits to data.

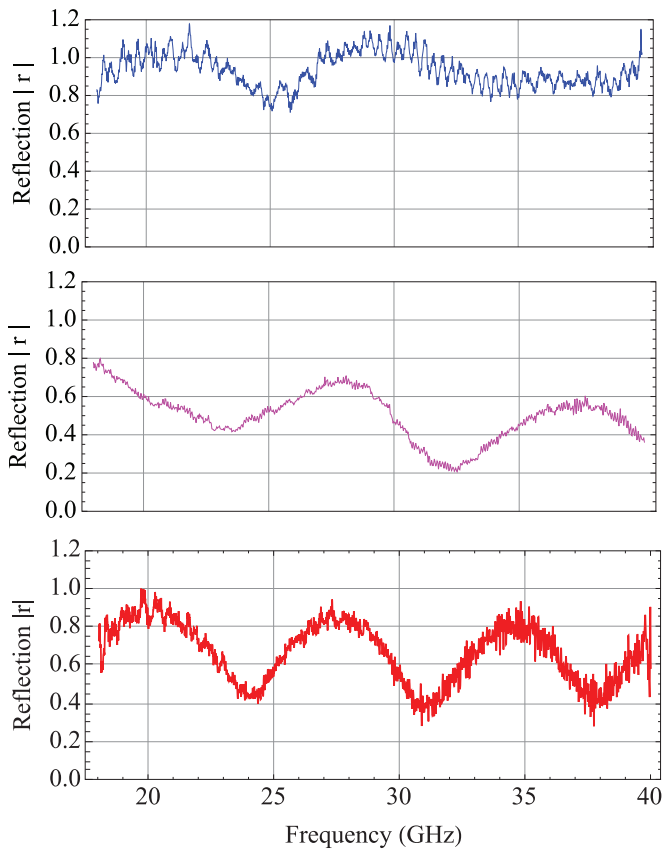

Fig. 3. Magnitude of the reflection coefficient as function of frequency for Lexan (*top*), paper (*middle*), and P1000 (*bottom*).

are configured as flat sheets, 15 × 30 cm, with parallel faces. In measurement, a metal plate backs the sample: this approximates, to first order, a human backdrop, which is similarly expected to be highly reflective [22]. The setup is shown in Fig. 1. A calibration procedure defines corrections to three terms in a one-port error model [9], [11] using S_{11} parameters for reflections from a metal plate at the reference plane, a metal plate offset 0.2–0.4 cm towards the horn, and an absorber. The use of a calibrated reference plane is different from standard FD-OCT, which uses an interferometer [23].

B. Data Collection

Data is collected for three materials: 1) polycarbonate plastic (Lexan); 2) paper (75 g/m^2 bond paper sheet, stacked); and 3) Primasheet 1000 (P1000), a PETN-based rubberized sheet explosive manufactured by Ensign-Bickford. The materials all have the nominal depth of 1–1.25 cm. The reflection in the time domain has a simple interpretation, as can be observed from Fig. 2, which shows the Fourier transform of the calibrated reflected spectrum. Relative to the calibration plane marked by time zero, there is an earlier reflection from the front surface, and a later large reflection from the reflective back layer. The second signal arrives after two passes across the sample, and its intensity varies according to absorption in the material. The total image contrasts of paper and P1000, as measured by the net energy reflected, are similar—30% and 50%, respectively.

The time-dependent reflection data can be analyzed to infer the refractive index, based on front surface reflectivity, time delay, net reflectivity, and phase [20], [24]–[26]. However, this approach has limitations. The arrival times of the peaks are resolved only to the precision of the inverse bandwidth. Moreover, modeling the time series data in terms of physical parameters is problematic because overlapping pulses need to be summed coherently. The usual approach to coherent superposition involves Fourier decomposition and application of geometric optics, and is thusly rooted in the frequency domain. Time-domain modeling also requires parameterization of the pulse shape. Applying the analysis to the frequency domain avoids these difficulties.

The reflection amplitude spectra for our three materials are shown in Fig. 3. Reflections of different orders interfere constructively and destructively to produce oscillations in frequency. Depending on the material, the interference peaks

occur with different frequency spacings, the max-to-min amplitude of reflectivity varies, and the mean reflectivity across frequency trends differently. Note that a reflection coefficient in Fig. 3 greater than unity is the result of calibration error (see Section III-A) or spread-loss effects [10]. Also, while the beam is directed in most part through the sample, diffraction on the sample edges may be adding to the reflection—particularly in the case of Lexan, which has sharp edges.

C. Parameter Fitting

The optical model is based on the physics of reflections from layered materials [27], which in the present case involve the layering of metal, sample, air, and two interfaces (the backing material and air are taken to be semi-infinite in extent). The total of the reflected electric field is a sum of the reflections escaping the slab, including internal reflections according to Fresnel's equations for transmission and reflection (see, for example, [28, Ch. 7.6.1]). The net reflection coefficient, r, defined as the ratio of the total reflected electric field to the incident field, is parameterized by ΔL, n', and n'', which are the sample thickness, the real component of the refractive index, and the imaginary component of the refractive index, respectively [6]. The values of the parameters are found numerically by fitting the wideband data to the model using a least squares optimization method. Normal incidence of ray paths at the surface interfaces is assumed. For nonmagnetic materials, the refractive index is given in terms of the relative permittivity, $n = \sqrt{\epsilon}$. The refractive index is assumed to be constant with frequency, unless conductivity is explicitly included (e.g., Section IV). The assumption of constant dielectric seems to be supported by measurement of military [29] and commercial explosives (Section IV). In event materials are encountered that show dielectric relaxation, this would be an added signature for material identification, which can be exploited by parameterizing with additional (Debye) fitting constants.

III. Results

A. Data Analysis

We are able to solve the reflectivity model parameters to fit the experimental data by the computational software in Mathematica [30], using the function *NonlinearModelFit*. The fitting is done on the complex data using the real part of r to find the parameters in Table I. The reflectivity fits are plotted on the phased reflectivity data in Fig. 4. The fitting parameters obtained from the real part apply as well to the imaginary part and the amplitude (see Fig. 4). Conversely, the fitting parameters can be determined from the imaginary part of r or from the reflection amplitude. Fitting to the complex components provide information on absolute phase, which relates to position relative to the calibration plane. The rows beneath the material parameters in Table I are measurement sensitivities, as discussed below.

The validity of the solutions for Lexan can be verified as an experimental control. Values reported by the manufacturer (SABIC) and [31] and [32] range from 1.658 to 1.667 for n', and 0.0038 to 0.0049 for n'', in agreement with our measurement.

TABLE I
Parameter Solutions and Errors

Material	ΔL (cm)	n'	n''
Lexan	1.262	1.676	0.006
A	±0.033	±0.003	±0.001
B	±0.007	±0.012	±0.006
C	±0.015	±0.012	±0.001
Paper	1.062	1.532	0.059
A	±0.006	±0.005	±0.003
B	±0.003	±0.003	±0.011
C	±0.007	±0.008	±0.001
P1000	1.290	1.690	0.031
A	±0.005	±0.003	±0.002
B	±0.001	±0.002	±0.007
C	±0.020	±0.020	±0.001

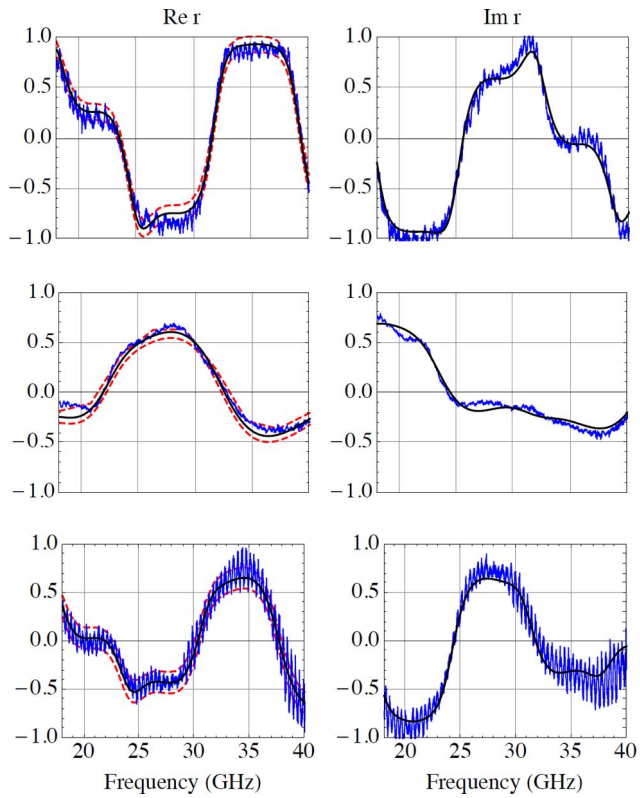

Fig. 4. Real and imaginary components of the reflection coefficient are shown with model solutions as solid lines for Lexan (*top*), paper (*middle*), and P1000 (*bottom*). Prediction confidence bands are indicated with dashed lines.

Errors are analyzed to demonstrate the efficacy of the dielectric detection. The refractive index and target thickness are derived quantities whose accuracy is determined by the measurement precision of the reflection coefficient (amplitude and phase), and the quality of the model fit. The amplitude error is estimated from the deviation of the reflection coefficient from unity when a metal plate is targeted, and is on the order of 0.06. The phase error is characterized by observing the effect of phase noise added to the model, and is on the order of 5°. The errors estimated from the variance in the reflection data are comparable with the instrumental precision, specified by Keysight for calibrated reflection measurement by the N5245A PNA-X as ±0.04

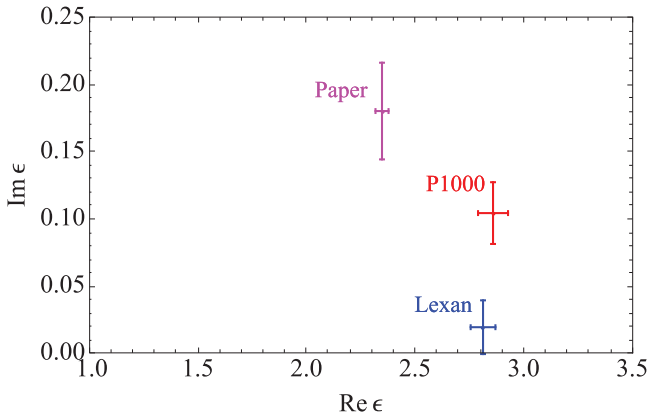

Fig. 5. Detected materials in dielectric space.

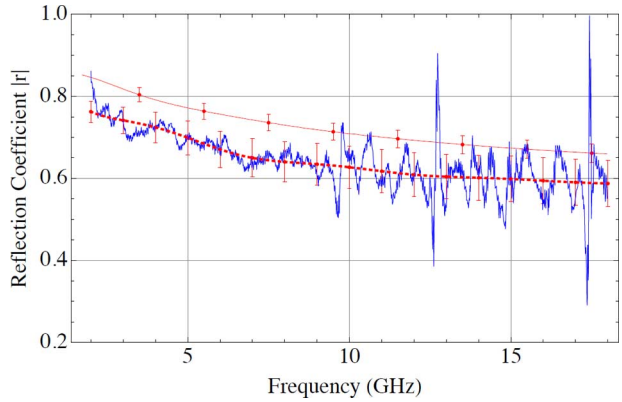

Fig. 6. Reflection coefficient of Dyno E-5. Dotted line is the functional fit to the free-space reflection data. Solid line is the reflection coefficient inferred from dielectric-probe measurement.

in magnitude and $\pm 2^\circ$ in phase at 26.5 GHz. The experimental phase measurement may include additional phase errors from surface irregularity, and variations in path length due to antenna illumination.

The measurement errors are propagated into the parameter errors by a Monte Carlo estimation technique, performing repeated numerical solution on data modified with simulated phase and amplitude errors. Each line A, B, and C in Table I correspond to the errors associated with the fitting model error, amplitude error, and phase error, respectively. The fitting model error on line A is derived from the confidence interval of the fitting algorithm, as exhibited in Fig. 4. The amplitude and phase errors on lines B and C are propagated from the measurement error estimates.

Data collection with the explosive was also repeated at 1/4, 1/2, and 3/4 of the thickness presented above. The mean and standard deviations of all four thickness were $n' = 1.73 \pm 0.03$ and $n'' = 0.038 \pm 0.10$, demonstrating that the detection is repeatable within margins specified by the measurement error.

B. Detection

In order to have practical application, the dielectric constants detected with millimeter-wave interrogation must be different enough to distinguish one from the other. This will depend on the separation of materials in the complex coordinate space defined by $\mathrm{Im}\,\epsilon$ and $\mathrm{Re}\,\epsilon$, as depicted in Fig. 5. This specificity will depend on the number of materials and the precision of measurement. The examples in Fig. 5 are substantially isolated so that they can, indeed, be distinguished. Identification could be accomplished by comparing the detected dielectric values with materials whose dielectric constants are known and provided for this purpose in a detection library [33], [34].

IV. Other Frequencies

The frequency band of 18–40 GHz, which encompasses current commercial systems, exhibits frequency-dependent reflection coefficient for weakly absorbing materials, as demonstrated above. However, commercial explosives, such as ammonium–nitrate (AN) and nitroglycerin (NG) slurries and gels, are less likely to be penetrable by millimeter waves in this band because their water content makes them highly absorptive. However, it is apparent that in a lower frequency band, 2–18 GHz, the reflection coefficient of these opaque materials changes with frequency because of electrical conduction. Although phenomenologically different from the signature in semi-transparent materials due to internal reflections, this frequency dependence due to conductivity can be analyzed using similar algorithms to extract dielectric constant.

As an example, Fig. 6 shows the reflection coefficient of Dyno E-5, an emulsion-type AN explosive manufactured by Dyno AP, as measured in the lower frequency band. Data was collected with the Agilent PNA-X network analyzer using a Q-par WBH2-18 wideband horn at a range of 17 cm from a 30.5 × 30.5 cm flat sample, of nominal thickness 0.9 cm, on a stainless-steel backing plate. It is evident from Fig. 6 that the spectrum does not show constructive interference from the front and back surface reflections, as in the previous examples. (An *a-posteriori* calculation shows that approximately 3% of the signal is due to reflection from the back surface.) The spectrum does show an increase in reflection coefficient towards the low end of frequencies, a variation that can be associated with conductivity. It can be demonstrated [35] that with a material obeying Ohm's law, $J = \sigma E$, the effective dielectric constant is

$$\epsilon = \epsilon' - j\epsilon'' - j\frac{\sigma}{2\pi f} \tag{1}$$

where the first two terms are the usual dielectric constant, and the third term adds the effect of conduction electrons.

To derive the dielectric constant, the reflection coefficient is fit as before to the Fresnel equation model, using σ as an additional free parameter. The solutions are tabulated in Table II. The errors are estimated from the confidence intervals provided by the fitting routine and sensitivity of the fitting parameters to variation in reflection data. The reflection coefficient for Dyno E-5 derived from the fitting parameters is plotted with the data in Fig. 6. Table II also presents the results from the measurement of paper (0.9 cm thick) in the 2–18-GHz band. Comparison of paper to the results above for 18–40 GHz show some differences, although the uncertainties are greater in the lower frequency band because of additional phase noise from phase-front variation and beam divergence across frequencies due to the proximity of the broadband horn [10]. The paper sample used was 24-lb sheet (90 g/cm^2), which differed from the previously

TABLE II
DETECTED DIELECTRIC CONSTANT 2–18 GHz

Material	ϵ'	ϵ''	$\sigma/2\pi\ (s^{-1})$	$\Delta L\ (cm)$
Dyno E-5	$11. \pm 6$	$3. \pm 3$	80 ± 20	0.86 ± 0.09
Paper	2.9 ± 0.3	0.31 ± 0.05	0.5 ± 0.3	0.96 ± 0.05

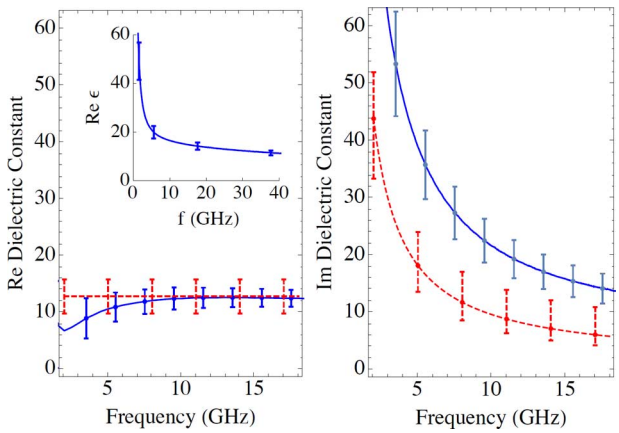

Fig. 7. Comparison of dielectric data for Dyno E-5 measured with probe (solid lines) and detected with free-space reflection (dashed lines). Inset is probe data before correcting probe polarization.

measured sample, so some difference may be inherent to the sample.

Fig. 7 compares the measurement of dielectric constant using the Agilent 85070E Performance Probe, and the free-space measurement from model fitting. The comparison shows the suitability of accounting for the imaginary component with the conductivity model. The real component is corrected for probe polarization using the method of [36]. The uncorrected probe data for 0.5–40 GHz, shown in the inset, exhibits probe polarization, but no sign of dielectric relaxation. Thus, the assumption of a fixed dielectric constant in the model is supported in this example by the probe data. The respective real dielectric constants are in good agreement, while the imaginary dielectric constants agree generally, to a much weaker confidence level.

V. DISCUSSION

The idealization of the experimental setup, and the assumptions in the optical model, are not inimicable for application to imaging systems. The assumption of normal incidence adopted here is not necessarily restrictive, as millimeter-wave imagers used at checkpoints scan a transmitter receiver linear array over a large aperture, with the effect to maximize the return at specular reflection [37]. The assumption of uniform permittivity over the band of detected frequencies was adequate for the discussed materials, and is likely to be valid for secondary high explosives as well, based on 1–18-GHz dielectric measurements [29]. Another assumption to the modeling is uniform layering. The image reconstruction will somewhat mitigate the effect of nonuniform layering by localizing the interrogating beam to smaller and more uniform cross sections of the target. At least in principle, the dielectric solutions can be done pixel by pixel. The finite angular beam from the transmitter antennas will also tend to moderate the effect of nonparallel surfaces, as it will broaden the angle for specular reflection, although the effect of ray path lengths due to angle may have to be considered.

A significant technical challenge to implementing the technique in personnel imaging systems is the human backdrop. The reflecting background can be replaced in the model by the appropriate value of refractive index, but assigning a value *a priori* is difficult because different areas of the skin will have different dielectric constant [17], and can vary from person to person as well. The background dielectric might be included as a free parameter for the fitting function, but another strategy is to infer the skin dielectric from nearby imaging, which does not include the target material.

In actual detection environments, the target configuration will also have additional complexities due to air gaps and clothing layers; these effects can be addressed by incorporating layered materials into the model, as needed.

Work that can advance the functionality of the technique includes: 1) demonstrating an imperfectly reflecting background, such as a flat surface with dielectric properties simulating skin [17]; 2) collimating and imaging optics to mitigate surface artifacts and thickness variation with less ideal objects; 3) employing multiple frequency bands to improve detection precision of materials across a large absorption parameter range; 4) expanding dielectric signatures to detect dielectric dispersion [23]; and 5) incorporating material and explosive measurement data into a dielectric space lookup table.

VI. CONCLUSION

The frequency content of data collected by AIT millimeter-wave imaging systems has been demonstrated to be useful for quantifying the dielectric constant of detected materials, an application that could facilitate the identification of concealed items on persons [38]. The detection is possible at small standoff distances in free space, as in existing screeners. The method presented here works in a broad range of frequencies in the band of 18–40 GHz, and exploits the constructive interference from multiple reflections and the energy loss in the ray paths traversing the sample. In opaque materials, which are likely to be conductive, the variation in reflection coefficient is apparent in a lower band of frequency, and is due to skin depth effects. In both cases, the complex dielectric constant is acquired using an optical model to fit the reflectivity spectrum.

ACKNOWLEDGMENT

The authors gratefully acknowledge the contributions of J. Greca, Battelle Memorial Institute, who collected the probe measurement data, P. R. Smith, Aaski Technology, who provided essential insights on probe polarization effects, and K. Babu, DHS/S&T/HSARPA/EXD.

REFERENCES

[1] R. A. Fenner, E. J. Rothwell, and L. L. Frasch, "A comprehensive analysis of free-space and guided-wave techniques for extracting the permeability and permittivity of materials using reflection-only measurements," *Radio Sci.*, vol. 47, no. 1, pp. RS1004:1–13, Feb. 2012.

[2] W. B. Weir, "Automatic measurement of complex dielectric constant and permeability at microwave frequencies," *Proc. IEEE*, vol. 62, no. 1, pp. 33–36, Jan. 1974.

[3] P. H. Tomlins and R. K. Wang, "Simultaneous analysis of refractive index and physical thickness by Fourier domain optical coherence tomography," *Proc. Inst. Elect. Eng.—Optoelectron.*, vol. 153, no. 5, pp. 222–228, Oct. 2006.
[4] U. C. Hasar, "A new microwave method based on transmission scattering parameter measurements for simultaneous broadband and stable permittivity and permeability determination," *Prog. Electromagn. Res.*, vol. 93, pp. 161–176, 2009.
[5] J. C. Weatherall, "Emission from dielectric materials at millimeter wavelengths in passive thermal environments," in *SPIE Defense, Security, and Sensing*. Bellingham, WA, USA: Int. Soc. Opt. Photon., 2010, p. 76700F.
[6] J. C. Weatherall, J. Barber, and B. T. Smith, "Identifying explosives by dielectric properties obtained through wide-band millimeter-wave illumination," in *SPIE Defense+ Security*. Bellingham, WA, USA: Int. Soc. Opt. Photon., 2015, p. 94620F.
[7] U. C. Hasar, J. J. Barroso, C. Sabah, and Y. Kaya, "Resolving phase ambiguity in the inverse problem of reflection-only measurement methods," *Prog. Electromagn. Res.*, vol. 129, pp. 405–420, 2012.
[8] D. K. Ghodgaonkar, V. V. Varadan, and V. K. Varadan, "A free-space method for measurement of dielectric constants and loss tangents at microwave frequencies," *IEEE Trans. Instrum. Meas.*, vol. 38, no. 3, pp. 789–793, Jun. 1989.
[9] M. H. Umari, D. K. Ghodgaonkar, V. V. Varadan, and V. K. Varadan, "A free-space bistatic calibration technique for the measurement of parallel and perpendicular reflection coefficients of planar samples," *IEEE Trans. Instrum. Meas.*, vol. 40, no. 1, pp. 19–24, Feb. 1991.
[10] K. Haddadi, M. M. Wang, O. Benzaim, D. Glay, and T. Lasri, "Contactless microwave technique based on a spread-loss model for dielectric materials characterization," *IEEE Microw. Wireless Compon. Lett.*, vol. 1, no. 19, pp. 33–35, Jan. 2009.
[11] M. Zhao, J. Shea, S. Hagness, and D. van der Weide, "Calibrated free-space microwave measurements with an ultrawideband reflectometer-antenna system," *IEEE Microw. Wireless Compon. Lett.*, vol. 16, no. 12, pp. 675–677, Dec. 2006.
[12] O. Tantot, M. Chatard-Moulin, and P. Guillon, "Measurement of complex permittivity and permeability and thickness of multilayered medium by an open-ended waveguide method," *IEEE Trans. Instrum. Meas.*, vol. 46, no. 2, pp. 519–522, Apr. 1997.
[13] M. E. Baginski, D. L. Faircloth, and M. D. Deshpande, "Comparison of two optimization techniques for the estimation of complex permittivities of multilayered structures using waveguide measurements," *IEEE Trans. Microw.Theory Techn.*, vol. 53, no. 10, pp. 3251–3259, Oct. 2005.
[14] I. Garcia-Ruiz, C. D. Aviles-Castro, H. Jardón-Aguilar, and J. Guerra-Vargas, "On the measurement of the complex permittivity of layers embedded in a multilayered dielectric material with the use of a free-space method," *Microw. Opt. Technol. Lett.*, vol. 33, no. 6, pp. 422–426, Jun. 2002.
[15] A. Elhawil, G. Koers, L. Zhang, J. Stiens, and R. Vounckx, "Comparison between two optimisation algorithms to compute the complex permittivity of dielectric multilayer structures using a free-space quasi-optical method in W-band," *IET Meas. Sci. Technol.*, vol. 3, no. 1, pp. 13–21, Jan. 2009.
[16] J. Barber, J. C. Weatherall, C. S. Brauer, and B. T. Smith, "Development of a contrast phantom for active millimeter-wave imaging systems," in *SPIE Defense, Security, and Sensing*. Bellingham, WA, USA: Int. Soc. Opt. Photon., 2011, p. 80190G.
[17] J. Barber, J. C. Weatherall, J. Greca, and B. T. Smith, "Toward the development of an image quality tool for active millimeter wave imaging systems," in *SPIE Defense + Security*. Bellingham, WA, USA: Int. Soc. Opt. Photon., 2015, p. 94620D.
[18] D. L. McMakin, P. E. Keller, D. M. Sheen, and T. E. Hall, "Dual-surface dielectric depth detector for holographic millimeter-wave security scanners," in *SPIE Defense, Security, and Sensing*. Bellingham, WA, USA: Int. Soc. Opt. Photon., 2009, p. 73090G.
[19] D. A. Andrews, N. D. Rezgui, S. E. Smith, N. Bowring, M. Southgate, and J. G. Baker, "Detection of concealed explosives at stand-off distances using wide band swept millimetre waves," in *SPIE Europe Security and Defence*. Bellingham, WA, USA: Int. Soc. Opt. Photon., 2008, p. 71170J.
[20] M. B. Abdillah, B. Lyons, and E. Entchev, "Identification of potential threat materials using active electromagnetic waves," U.S. Patent 8390504, Mar. 5, 2013.
[21] D. M. Sheen, D. L. McMakin, T. E. Hall, and R. H. Severtsen, "Real-time wideband cylindrical holographic surveillance system," U.S. Patent 5,859,609, Jan. 12, 1999.
[22] S. I. Alekseev and M. C. Ziskin, "Human skin permittivity determined by millimeter wave reflection measurements," *Bioelectromagnetics*, vol. 28, no. 5, pp. 331–339, Jul. 2007.
[23] W. V. Sorin and D. F. Gray, "Simultaneous thickness and group index measurement using optical low-coherence reflectometry," *IEEE Photon. Technol. Lett.*, vol. 4, no. 1, pp. 105–107, Jan. 1992.
[24] S. Ahmed, O. Ostwald, and L. Schmidt, "Automatic detection of concealed dielectric objects for personnel imaging," in *IEEE MTT-S Int. Microw. Workshop Wireless Sensing, Local Positioning, RFID*, Cavtat, Croatia, Sep. 2009, pp. 1–4.
[25] A. Luukanen *et al.*, "Multi-band imaging and adaptive beam-steering techniques for the submillimetre-wave range," in *7th Eur. Conf. Antennas Propag.*, Göteborg, Sweden, Aug. 2013, pp. 1946–1948.
[26] S. Jaruwatanadilok, Y. Kuga, and A. Ishimaru, "An electromagnetic model for plastic composite materials under obscuring layers," in *IEEE Int. Antennas Propag. Symp.*, Singapore, Nov. 2006, pp. 4841–4844.
[27] G. B. Airy, "On the phenomena of Newton's rings when formed between two transparent substances of different refractive powers," *Phil. Mag.*, vol. 2, no. 7, pp. 20–30, Jan. 1833.
[28] M. Born and E. Wolf, *Principles of Optics: Electromagnetic Theory of Propagation, Interference and Diffraction of Light*. Cambridge, U.K.: Cambridge Univ. Press, 1999.
[29] A. L. Higginbotham Duque, W. L. Perry, and C. M. Anderson-Cook, "Complex microwave permittivity of secondary high explosives," *Propell. Explos. Pyrot.*, vol. 39, no. 2, pp. 275–283, Apr. 2014.
[30] *Mathematica Edition: Version 9.0.*. Champaign, IL, USA: Wolfram Res. Inc., 2012.
[31] W. B. Westphal and A. Sils, "Dielectric constant and loss data," Dept. Commerce, Nat. Telecommun. Info. Service, Wright Patterson Air Base, OH, USA, Tech. Rep. AFML-72–39, 1972.
[32] P. I. Dankov, V. P. Levcheva, and V. N. Peshlov, "Utilization of 3D simulators for characterization of dielectric properties of anisotropic materials," in *Eur. Microw. Conf.*, Paris, France, Oct. 2005, pp. 1–4.
[33] J. Barber, J. C. Weatherall, B. T. Smith, S. Duffy, S. J. Goettler, and R. A. Krauss, "Millimeter wave measurements of explosives and simulants," in *SPIE Defense, Security, and Sensing*. Bellingham, WA, USA: Int. Soc. Opt. Photon., 2010, p. 76700E.
[34] J. C. Weatherall, J. Barber, C. S. Brauer, and B. T. Smith, "Measurement of the reflectivity and absorptivity of liquids, powders, and solids at millimeter wavelengths using dielectric detection by a resonator-post fixture between parallel conducting plates," in *SPIE Defense, Security, and Sensing*. Bellingham, WA, USA: Int. Soc. Opt. Photon., 2011, p. 80190F.
[35] J. D. Jackson, *Classical Electrodynamics*. New York, NY, USA: Wiley, 1999.
[36] F. Arroyo, F. Carrique, T. Bellini, and A. Delgado, "Dielectric dispersion of colloidal suspensions in the presence of stern layer conductance: Particle size effects," *J. Coloid Interf. Sci.*, vol. 210, no. 1, pp. 194–199, Feb. 1999.
[37] D. M. Sheen, D. L. McMakin, and T. E. Hall, "Three-dimensional millimeter-wave imaging for concealed weapon detection," *IEEE Trans. Microw. Theory Techn.*, vol. 49, no. 9, pp. 1581–1592, Sep. 2001.
[38] B. T. Smith, J. C. Weatherall, and J. B. Barber, "Method for identifying materials using dielectric properties through active millimeter wave illumination," U.S. Patent 8,946,641, Feb. 3, 2015.

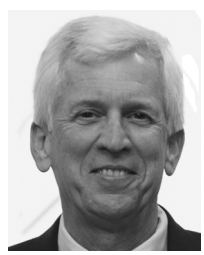

James C. Weatherall received the B.S. degree from the California Institute of Technology, Pasadena, CA, USA, in 1975, and the Ph.D. degree in plasma physics from the University of Colorado, Boulder, CO, USA in 1980.

From 1982 to 1984, he was a National Academy of Sciences, National Research Council Research Associate with the NASA Goddard Space Flight Center. From 1984 to 1992, he was with General Dynamics, Pomona, CA, USA, where he was involved in the development of high-power microwave sources. From 1992 to 2002, he was an Associate Professor of astrophysics with the New Mexico Institute of Mining and Technology. He is currently a Senior Research Scientist with the Critical Infrastructure Business Unit, Transportation Security, Battelle Memorial Institute, Egg Harbor Township, NJ, USA. His research has applied to electromagnetic technology for detection of explosives.

Dr. Weatherall is a Member of the American Physical Society.

Jeffrey Barber received the B.S. degree from Allegheny College, Meadville, PA, USA, in 1998, and the Ph.D. degree from Oregon State University, Corvallis, OR, USA, in 2003.

From 2003 to 2005, he was an Agnew National Security Postdoctoral Fellow with the Los Alamos National Laboratory, Los Alamos, NM, USA, where he performed terahertz-time domain spectroscopy and Raman spectroscopy on explosives. He is currently a Senior Research Scientist with the Critical Infrastructure Business Unit, Transportation Security, Battelle Memorial Institute, Egg Harbor Township, NJ, USA. His research is related to the detection of explosives via various electromagnetic techniques.

Barry T. Smith received the B.S. degree from Duquesne University, Pittsburgh, PA, USA, in 1972, and Ph.D. degree in physics from the College of William and Mary, Williamsburg, VA, USA, in 1978.

He is currently with the U.S. Department of Homeland Security, Science and Technology Directorate, Transportation Security Laboratory, William J. Hughes Technical Center, Atlantic City International Airport, Atlantic City, NJ, USA. His current responsibilities include the research and development of systems to detect explosives and weapons concealed on personnel at checkpoint in aviation, mass transit, and public venues. He also manages the Electromagnetic Signatures of Explosives Laboratory for the measurement of explosive material properties from dc to THz. His current interests include millimeter waves and laser spectroscopy.

Dr. Smith is a Member of the American Physical Society.